ACS APPLIED MATERIALS & INTERFACES

Research Article

www.acsami.org

High-Efficiency Small Molecule-Based Bulk-Heterojunction Solar Cells Enhanced by Additive Annealing

Lisheng Li,[†] Liangang Xiao,[†] Hongmei Qin,[†] Ke Gao,[†] Junbiao Peng,[†] Yong Cao,[†] Feng Liu,[*,‡] Thomas P. Russell,[‡] and Xiaobin Peng[*,†]

[†]Institute of Polymer Optoelectronic Materials and Devices, State Key Laboratory of Luminescent Materials and Devices, South China University of Technology, 381 Wushan Road, Guangzhou 510640, China

[‡]Materials Sciences Division, Lawrence Berkeley National Laboratory, Berkeley, California 94720, United States

Supporting Information

ABSTRACT: Solvent additive processing is important in optimizing an active layer's morphology and thus improving the performance of organic solar cells (OSCs). In this study, we find that how 1,8-diiodooctane (DIO) additive is removed plays a critical role in determining the film morphology of the bulk heterojunction OSCs in inverted structure based on a porphyrin small molecule. Different from the cases reported for polymer-based OSCs in conventional structures, the inverted OSCs upon the quick removal of the additive either by quick vacuuming or methanol washing exhibit poorer performance. In contrast, the devices after keeping the active layers in ambient pressure with additive dwelling for about 1 h (namely, additive annealing) show an enhanced power conversion efficiency up to 7.78% with a large short circuit current of 19.25 mA/cm^2, which are among the best in small molecule-based solar cells. The detailed morphology analyses using UV-vis absorption spectroscopy, grazing incidence X-ray diffraction, resonant soft X-ray scattering, and atomic force microscopy demonstrate that the active layer shows smaller-sized phase separation but improved structure order upon additive annealing. On the contrary, the quick removal of the additive either by quick vacuuming or methanol washing keeps the active layers in an earlier stage of large scaled phase separation.

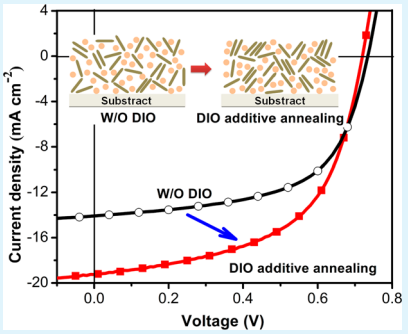

KEYWORDS: *inverted organic solar cells, additive annealing, morphology, small molecule, porphyrin*

1. INTRODUCTION

Bulk heterojunction (BHJ) organic solar cells (OSCs) have attracted much attention in both academia and industry for their potential in producing large-scale, lightweight, flexible, and low-cost solar cell panels.[1−5] Small molecules (SMs) are promising photovoltaic materials, showing unique advantages such as high purity, well-defined chemical structure, and high synthetic reproducibility.[6−9] Also the power conversion efficiencies (PCEs) of SM-based solar cells have improved significantly up to 10% comparable to those of BHJ polymer counterparts[10−12] through the synergic optimizations of material's chemical structures and device engineerings.[13,14] Recently, we employed an A-π-D-π-A strategy to synthesize porphyrin-based OPV materials first, and high power conversion efficiencies have been achieved along with other groups,[15−19] demonstrating that porphyrins are promising on organic solar cells.

To achieve a high performance OSC, good film morphology with suitable nanostructured phase separation and well-established donor/acceptor networks is necessary.[20−25] Among various processing methods in controlling BHJ film morphology, solvent additive is very useful[26−32] and 1,8-diiodooctane (DIO) is widely used as a solvent additive. Because DIO shows much higher boiling point than the main solvent such as chlorobenzene (CB) and is usually poorer for polymer dissolvation but good for [6,6]-phenyl C_{61}-butyric acid methyl ester (PCBM), during the solvent removal when a device is fabricated, the ratio of DIO additive gradually increases, inducing the easier aggregation of polymer donors than PCBM. Therefore, the residual DIO within the "dried" BHJ layer can still affect the film morphology,[33,34] and it has been reported that the residual DIO should be removed immediately after the active layer's deposition in order to obtain higher performance devices in a conventional structure.[35]

Recently, we reported that the BHJ OSCs in a conventional structure based on 5,15-bis(2,5-bis(2-ethyl-hexyl)-3,6-dithienyl-2-yl-2,5-dihydro-pyrrolo 3,4-c]pyrrole-1,4-dione-5′-yl-ethynyl)-10,20-bis(4-octyloxy-phenyl)-porphyrin zinc (DPPEZnP-O) and PCBM delivered us a PCE of 7.23% when DIO additive was used.[16] Since OSCs in inverted structures show more advantages,[5,36−39] BHJ OSCs based on DPPEZnP-O in an inverted structure are fabricated in this study, and we notice that how DIO is removed from the active layers plays a critical role in determining the film morphology. We see that the quick removal of the additive either by quick vacuuming or methanol solvent washing keeps the active layers in an earlier stage of

Received: July 23, 2015
Accepted: September 10, 2015
Published: September 10, 2015

DOI: 10.1021/acsami.5b06691
ACS Appl. Mater. Interfaces 2015, 7, 21495−21502

Scheme 1. Molecular Structures of DPPEZnP-O and PCBM and the Structure of Inverted OSC Devices

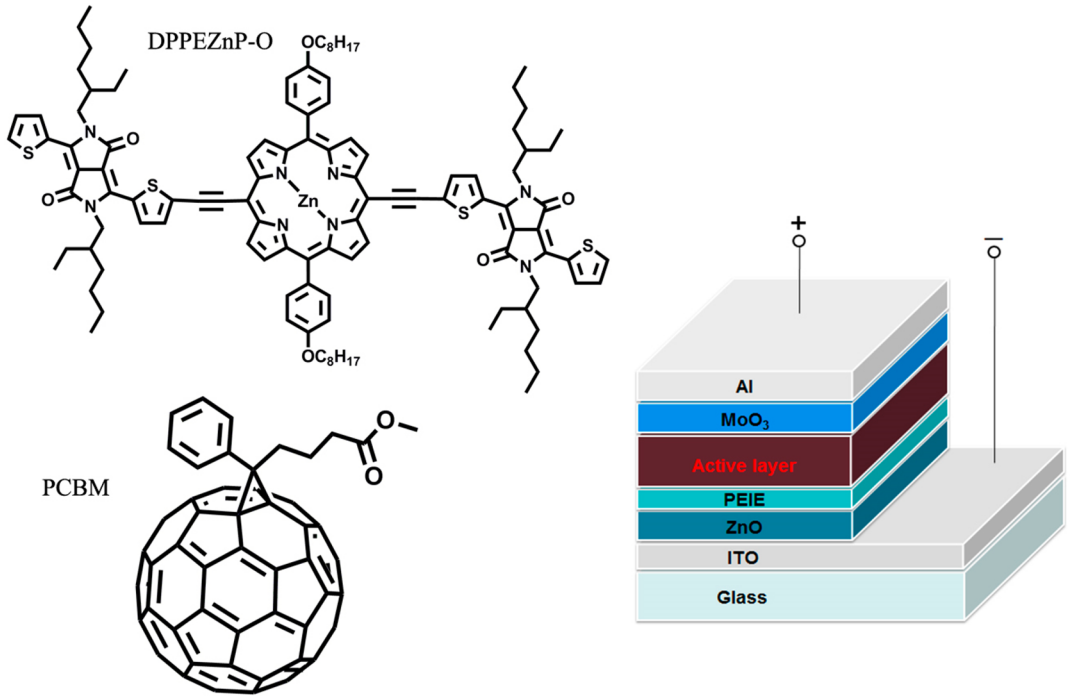

large-scaled phase separation. On the contrary, keeping DIO in active layer in ambient pressure for a period of time (additive annealing) helps build up a smaller sized phase separation with more ordered DPPEZnP-O in blend films, leading to the PCE enhancement up to 7.78% with a very high short circuit current (J_{SC}) of 19.25 mA cm^{-2}.

2. RESULTS AND DISCUSSION

Scheme 1 shows the molecular structures of DPPEZnP-O and PCBM and the inverted device structures used, respectively, in this study. The donor molecule is featured with a porphyrin ring in the center, two diketopyrrolopyrrole units at both sides, and two ethylene linkages in between. This combination leads the molecule flat and therefore highly conjugated to help π-electrons' delocalization and intermolecules' cofacial packing. The $J-V$ curves and performance of the BHJ OSCs using different additive contents in inverted device structures are shown in Figure 1 and Table 1. A PCE of 6.14% was obtained

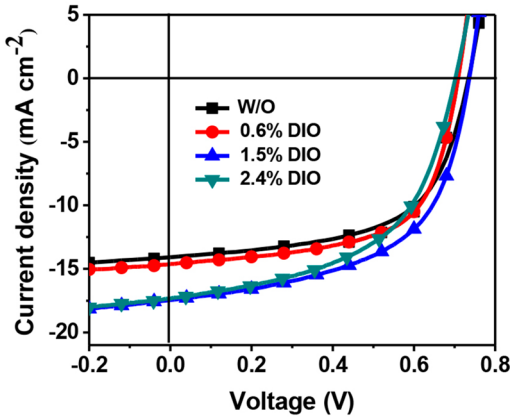

Figure 1. $J-V$ curves of inverted OSCs using different amounts of DIO additive.

Table 1. Device Performance Using Different Amount of DIO Additive

additive	J_{SC}[a] (mA cm^{-2})	V_{OC}[b] (V)	FF[a] (%)	PCE (%)[a]
W/O DIO	14.07 (13.82 ± 0.33)	0.74	58.96 (58.29 ± 0.73)	6.14 (6.01 ± 0.18)
0.6% DIO	14.60 (14.21 ± 0.45)	0.71	62.37 (61.40 ± 0.94)	6.46 (6.27 ± 0.23)
1.5% DIO	17.45 (17.00 ± 0.53)	0.74	55.91 (55.30 ± 0.84)	7.22 (6.94 ± 0.28)
2.4% DIO	17.35 (16.89 ± 0.63)	0.70	53.37 (52.85 ± 0.63)	6.50 (6.34 ± 0.26)

[a]Maximum values, and average values with standard deviation given in parentheses. [b]Almost no deviation.

when processed from pure CB. Adding DIO additive improved the J_{SC}, but showing a plateau when 1.5 v % DIO was used. Further increasing DIO content led to the decrease of fill factors (FF), and thus reduced the PCEs. Also the best device using 1.5% DIO additive showed a PCE of 7.22% (open circuit voltage (V_{OC}) = 0.74 V, J_{SC} = 17.45 mA cm^{-2}, and FF = 55.91%).

During the fabrication of the above devices, as soon as the BHJ films were spin-coated they are quickly transferred into a vacuum chamber to remove the DIO residue under a high vacuum about 0.1 Pa, which is named quick vacuuming in here. Since it was reported that the residual DIO within the "dried" BHJ film after spin-coating still can affect the film morphology and the residual DIO should be removed immediately after the deposition in order to obtain a higher device performance,[33,34] we washed the DIO residue away with a small amount of methanol right after the active layers were spin-casted (defined as solvent washing in here). However, different from the reported cases of improved device performance,[35] a lower PCE of 6.41% with a reduced J_{SC} of 15.77 mA cm^{-2} and a similar FF of 54.91% was obtained for our inverted OSCs. Therefore, the spin-coated BHJ active layers were stored at ambient

DOI: 10.1021/acsami.5b06691
ACS Appl. Mater. Interfaces 2015, 7, 21495−21502

temperature and pressure for tens of minutes (namely, additive annealing) before being transferred to a vacuum chamber for drying, and the OSCs showed improved performance and the best performance was achieved upon the additive annealing for about 1 h with enhanced values of J_{SC}, FF, and PCE up to 19.25 mA cm^{-2}, 56.10% and 7.78%, respectively. Shown in Figure 2 and Table 2 are the OSC results of different additive-handlings of the active layers.

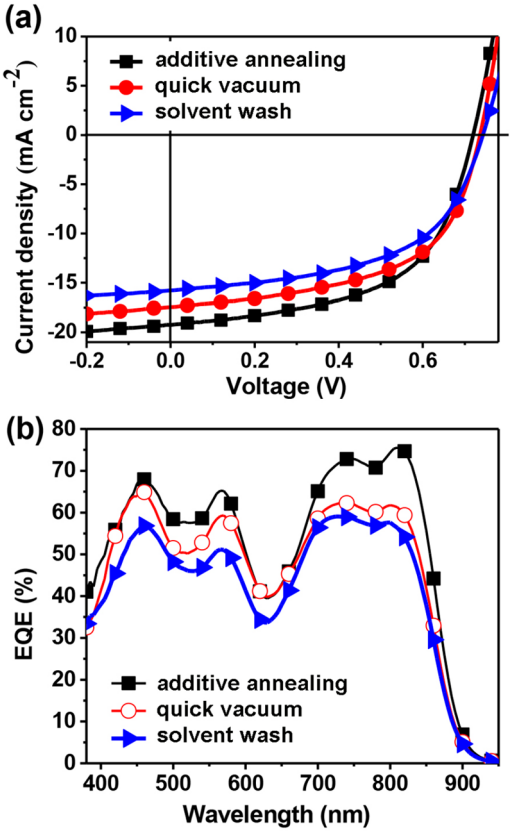

Figure 2. (a) J–V characteristics of the inverted OSC devices based on DPPEZnP-O/PCBM (1.5% DIO) upon additive annealing, quick vacuuming, and methanol solvent washing. (b) The EQE curves of the corresponding devices.

It is known that FF and the J_{SC} values are sensitive to series resistance (R_S) for an OSC.[40] In line with the enhancement of FF and J_{SC}, the R_S values calculated from the slopes of the J–V curves near J = 0 mA cm^{-2} for quick vacuumed and methanol solvent washed devices are 5.25 and 7.81 Ω cm^2, respectively, both higher than that of additive annealed devices (4.68 Ω cm^2). Furthermore, as shown in Figure 2b, additive annealed devices show higher external quantum efficiencies (EQE) in the whole range from 380 to 900 nm, particularly in the near-infrared region (700–900 nm). As discussed below, such significant enhancement in EQE gives rise to an enhanced J_{SC} in devices, which can be ascribed to the morphology improvement after the additive annealing.

The carrier mobilities of the BHJ thin films were investigated by constructing organic field-effect transistors (OFETs) and single carrier devices (hole-only devices fabricated in the configuration of indium tin oxide (ITO)/(3,4-ethylenedioxythiphene):poly(styrenesulfonate) (PEDOT:PSS)/active layer/MoO3/Al) using space charge limited current (SCLC) method. Shown in Figure 3 are the transfer curves

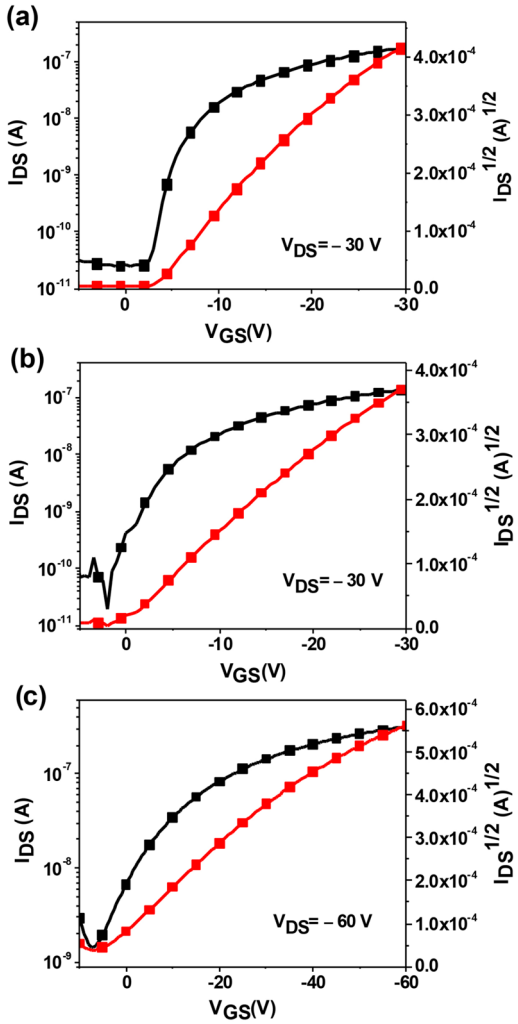

Figure 3. Transfer characteristics of the unencapsulated OFET device based on DPPEZnP-O/PCBM (1.5% DIO) BHJ films under (a) additive annealing, (b) quick vacuuming, and (c) methanol solvent washing. The carrier mobilities are obtained from saturation regions.

of bottom gate/top contact OFET devices using 300 nm SiO_2 as dielectrics. The hole mobilities of the BHJ blends upon

Table 2. Device Performance Using Different Additive Removal Methods

conditions	J_{SC}[a] (mA cm^{-2})	V_{OC}[b] (V)	FF[a] (%)	PCE (%)[a]	R_S[c] (Ω cm^2)
additive annealing	19.25(18.98 ± 0.36)	0.72	56.10(55.64 ± 0.85)	7.78 (7.64 ± 0.17)	4.68
quick vacuuming	17.45(17.12 ± 0.48)	0.74	55.91(55.24 ± 0.99)	7.22 (6.94 ± 0.28)	5.25
solvent washing	15.77(15.32 ± 0.73)	0.74	54.91(54.24 ± 1.29)	6.41 (6.18 ± 0.35)	7.81

[a]Maximum values, and average values with standard deviation given from more than 10 devices in parentheses. [b]Almost no deviation. [c]R_S was estimated from the device with the maximum PCE.

DOI: 10.1021/acsami.5b06691
ACS Appl. Mater. Interfaces 2015, 7, 21495–21502

different DIO removal procedures are summarized in Table 3. Quick vacuumed thin-films show a medium hole-mobility of

Table 3. Hole Motilities Measured Using OFETs and SCLC Method

processing condition	μ_{FET} ($cm^2\ V^{-1}s^{-1}$)	μ_{SCLC} ($cm^2\ V^{-1}s^{-1}$)
additive annealing	1.36×10^{-3}	8.12×10^{-4}
quick vacuum	8.92×10^{-4}	3.19×10^{-4}
solvent wash	3.64×10^{-4}	2.82×10^{-4}

8.92×10^{-4} $cm^2\ V^{-1}\ s^{-1}$, methanol solvent washed samples show a lowest hole-mobility of 3.64×10^{-4} $cm^2\ V^{-1}\ s^{-1}$, and additive annealed samples show the highest hole-mobility up to 1.36×10^{-3} $cm^2\ V^{-1}\ s^{-1}$. In SCLC measurements, the trend of mobility changes agrees well with the OFET results, showing that additive annealing leads to the hole-mobility enhancement in both horizontal and vertical direction with respect to the sample surface. Also this improvement originates from a better crystalline order of DPPEZnP-O that will be characterized in detail in the following discussions.

In order to understand how the different handlings of additive removal affect the device performance, we first performed UV−vis-NIR measurements on the BHJ films. As shown in Figure 4, BHJ thin films without using DIO show a

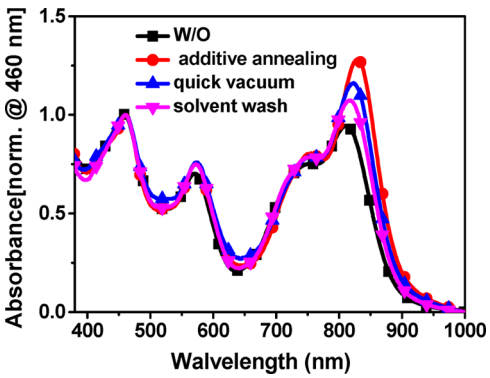

Figure 4. UV−vis-NIR absorption spectra for BHJ films of DPPEZnP-O/PCBM without DIO and with 1.5% DIO (v/v, DIO/CB) under additive annealing, quick vacuuming, and methanol solvent washing.

broad absorption from 400 to 900 nm. NIR region from 650 to 900 nm is of the most interest, featuring with two peaks at ∼750 and ∼810 nm. When DIO additive was used, the peak at ∼810 nm shifts to longer wavelength region, and this peak bathochromic-shifts gradually finally to 830 nm with its intensity increasing steady from solvent washed, quick vacuumed to additive annealed films. The red-shifting and growing of this long wavelength peak indicate a more ordered solid-state packing of aromatic molecules and thus the electronic communication between intermolecular stacks improves.[41−43] The more ordered structures can lead to a more balanced charge transport, contributing to the fill factor improvement. The long-wavelength peak for quick vacuumed sample shows a peak position in-between those of solvent washed and solvent annealed films, further conforming the importance of additive dwelling in morphology control since it takes more time to remove DIO for the quick vacuumed films than the solvent washed ones.

The molecular packing in BHJ blend films was studied by the grazing incidence X-ray diffraction (GIXD) method. Shown in Figure 5a are the diffractograms of the samples upon different additive removal procedures. Also the corresponding in-plane and out-of-plane line-cut profiles are summarized in Figure 5b,c. For the conventional quick vacuumed samples, one broad diffraction ring at 1.3−1.6 $Å^{-1}$ is seen, coming from the combination of PCBM diffraction and DPPEZnP-O $\pi-\pi$ stacking. The strong overlap of these two features makes it hard for further analyzing. In the low q region, a broad hump is seen from 0.2 to 0.4 $Å^{-1}$, coming from the alkyl−alkyl interaction that forms in the (100) crystalline direction. Such a broad peak with low intensities indicates the structure order in this direction is poor and there is strong wiggling when molecules start to order. Also the large π surface of DPPEZnP-O enhances the cofacial stacking and thus slight deviations in crystals can be tolerated. The (200) peak is also observed for this sample, indicating a good statistical persistence of crystals. Methanol solvent washed samples show a similar crystalline order compared to quick vacuumed ones. A slight enhancement of the (100) peak in the in-plane direction indicates a slightly preferred face-on orientation. Additive annealed thin films show drastically different crystalline behaviors. Two sharp peaks show up in 0.2−0.4 $Å^{-1}$ region, one located at 0.245 $Å^{-1}$ (2.56 nm) and the other at 0.33 $Å^{-1}$ (1.9 nm). High ordered peaks are also obtained in corresponding q spacing. The sharp peak intensity and reduced peak width for both indicate much better crystallinity and crystalline order. Combining the scattering signals with the molecular chemical structure, two different packing motifs are proposed for DPPEZnP-O as shown in Figure 5d,e. The alkoxyl-to-alkoxyl chain interaction gives rise to the long distance packing; and the sliding of molecules leads to ethyhexyl-to-ethyhexyl chain interaction and gives rise to the short distance packing. In peak analysis, the 0.245 $Å^{-1}$ peak gives an area of 62.8 au and a full-with-at-half-maximum (fwhm) of 0.0295, thus the crystal size is calculated to be 21 nm. The 0.33 $Å^{-1}$ peak gives an area of 51.2 au and a fwhm of 0.0647, corresponding to a crystal size of 9.7 nm. Thus, we can conclude that longer distance stacking exists with larger crystal size for solvent annealed samples and the broad peak for quick vacuumed and methanol solvent washed samples can be a summation of the two peaks. The longer dwelling time of DIO molecules inside BHJ blends induces crystal perfection by driving the intermediate states (complicated alkyl chain interactions) to the two preferred stacking modes. The peak intensity and shape of the 1.3−1.6 $Å^{-1}$ scattering remain similar in all the three cases, indicating that the aggregation of PCBM does not change much when the residual DIO in the blend films was removed by different methods. It should be noted that a small molecule is fractions of a linear polymer chain. Though it is simpler in chemical structure, the orientation and molecular interactions can be much more complicated compared to polymer counterparts. For example, when a different side chain is used, different side chain interactions need to be considered, and molecule side-to-side interactions need to be considered too. As shown in this study, the longer dwelling of additive in small molecule blends can be a new handle to control molecular organizations and phase separations, which is an analogue to solvent vapor annealing but with much simplified experimental handling.

The length scale of phase separation is another critical parameter determining the performance of OSCs. We probed this feature using resonant soft X-ray scattering methods by taking advantage of the high contrast and large probe length scales of low wavelength photons. BHJ thin films were floated

DOI: 10.1021/acsami.5b06691
ACS Appl. Mater. Interfaces 2015, 7, 21495−21502

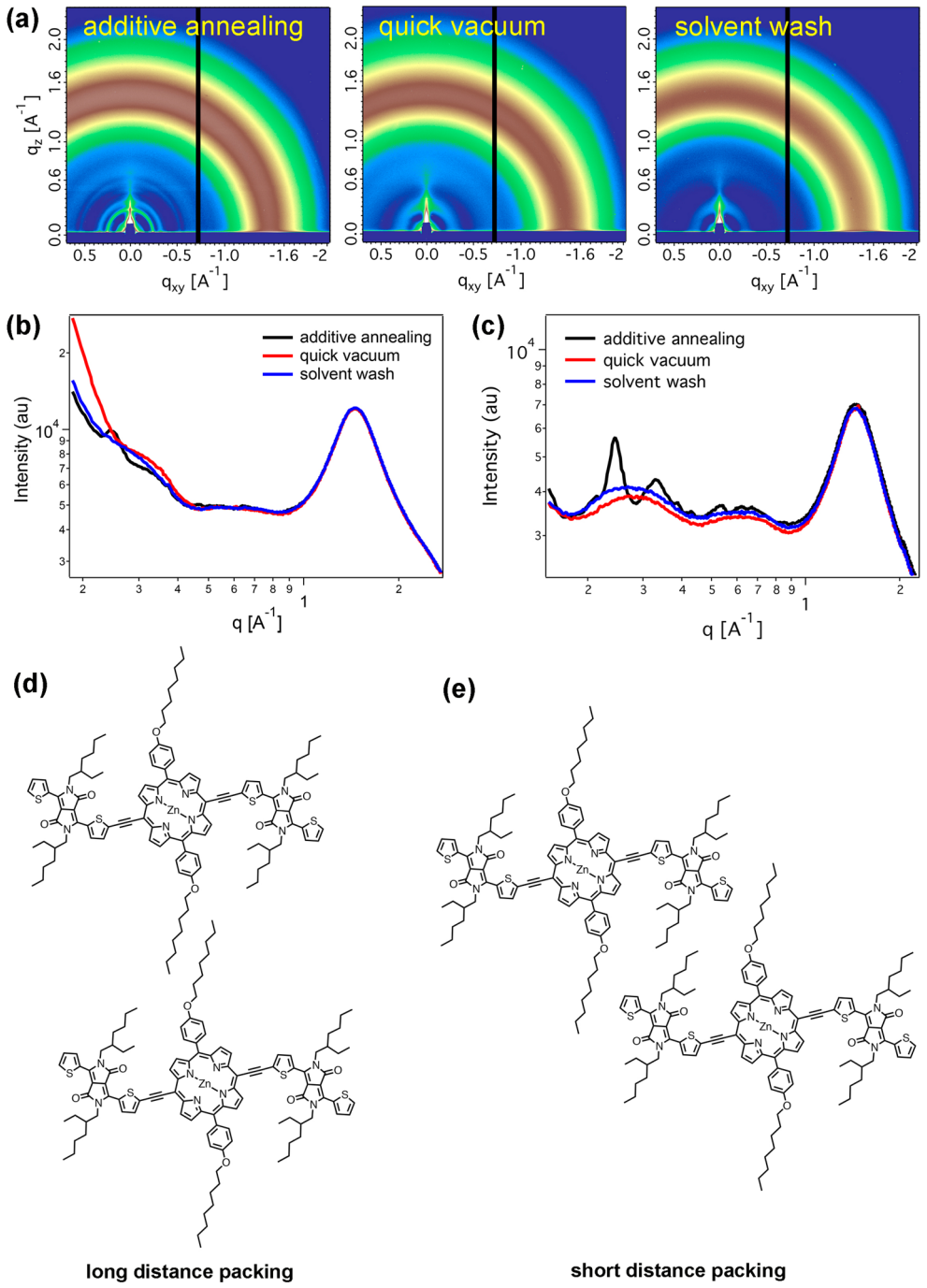

Figure 5. (a) GIXD diffraction images of DPPEZnP-O/PCBM blends processed from different recipes; (b) in-plane and (c) out-of-plane line cut profiles of GIXD data; (d and e) two different packing motifs of DPPEZnP-O molecules in blends.

onto silicon nitride window and experiments were carried out in transmission mode. The scattering profiles are plotted in Figure 6. For quick vacuumed samples, a strong diffraction peak shows up in 0.003 $Å^{-1}$, giving a phase separation size of 209 nm, which should originate from PCBM aggregations. Besides the major scattering peak, a shoulder at 0.012 $Å^{-1}$ is seen, corresponding to a distance of 52 nm. Thus, in this system, a multilength scaled morphology exists. For these devices, a 17.45 mA/cm^2 current density and 7.22% PCE were obtained, which are quite high in deep absorbing low band gap materials, and the 52 nm phase separation is key to generate such a large current. For methanol washed samples, the scattering peak slightly moves to higher q (0.0032 $Å^{-1}$), giving a distance of 196 nm. Similar high q scattering around the 50 nm size feature is also seen. In the very low q region (0.002 $Å^{-1}$), the intensity increases, indicating the growth of some even large features, which go out of the length scale that RSoXS can probe. The growth of large size feature can be the key for the reduced J_{SC} for the methanol solvent washed OSCs. Additive annealing leads to drastic changes in RSoXS. The major scattering peak in quick vacuumed sample reduces by a half of the intensity, and in the extreme low q region, new features grow up as in methanol washed samples, and the intensity grows up quickly. It is suspected that coalescence of domains under the presence of DIO leads to a larger domain and thus gives rise to the turning up in low q intensity. This process should be

DOI: 10.1021/acsami.5b06691
ACS Appl. Mater. Interfaces 2015, 7, 21495−21502

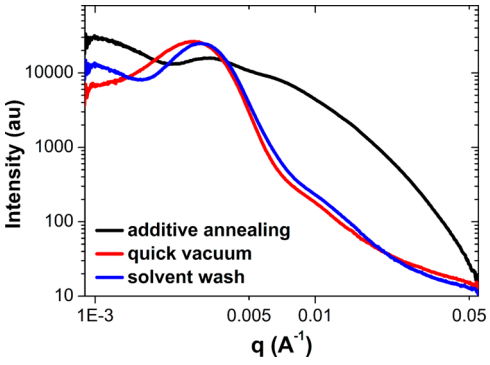

Figure 6. RSoXS profiles of DPPEZnP-O/PCBM blends processed from 1.5% DIO−CB solvent mixtures under different drying procedures.

detrimental to the device performance yet with the extent we cannot estimate at this point. A more pronounced feature is observed in the high q region. A broad hump is seen from 0.007 to 0.05 Å^{-1}, and thus a continuous length scale of phase separation from tens to hundreds of nanometers exists in this case. The finite phase separation helped with light extraction and thus elevated J_{SC} and EQE in whole spectrum are seen. In previous discussion we saw that additive annealing leads to enhanced crystallinity of the BHJ film and gives better-defined crystal structures. The 10 nm and 21 nm of the (100) crystal size are seen in GIXD measurements, and dispersion of these crystals inside a PCBM rich matrix could give the length scale of phase separation in RSoXS. It is thus plausible to state that the growth of DPPEZnP-O crystallites forms one domain and thus determines the length scale of phase separation. The improved J_{SC}, hole mobility, and fill factor for the OSCs upon additive annealing are the direct consequences of the better-sized phase separation, the improved crystallinity, and reduced charge recombination.

The surface features of BHJ blends using different additive removal procedures were also investigated by atomic force microscopy (AFM). As shown in Figure 7, the quick vacuumed sample gives features of hundreds of nanometers, which is similar to many previous reports of strong PCBM aggregated BHJ blends. Methanol washing changes the thin film's topology but still with large size scaled domains, agreeing well with RSoXS characterizations. Additive annealed thin film does not show well-defined surface features of hundreds of nanometers. Some irregular large domains exist, and their interdistance gave rise to the low q feature in RSoXS. It should also be noted that surface roughness for additive annealed sample increases, giving a RMS roughness of 9.8 nm. In comparison, quick vacuumed and methanol washed samples show smaller RMS roughness of 8.0 and 2.2 nm, respectively.

3. CONCLUSION

In conclusion, the performance for porphyrin small molecule-based OSCs in inverted structure was enhanced with an good PCE up to 7.78% and a very large J_{SC} of 19.25 mA cm^{-2} upon DIO additive annealing for about 1 h in ambient pressure before moved to a vacuum chamber for drying. Compared to conventional removal of additive by quick vacuuming and methanol washing, additive annealing treatment improves the ordering of donor molecules and the growth of crystallites with small length scaled phase separation (<100 nm) in BHJ blend films leads to the formation of better crystalline domains. The connected domain-networks with small length scaled phase separation form an important platform to split excitons and conduct charge carriers and thus contribute largely to the improved J_{SC} that a device can deliver. Physical process of additive annealing is similar to slow spin-coating and subsequent solvent vapor annealing for OSCs, which both give rise to enhanced crystallinity and device currents, but additive annealing shows more flexibility in fine-tuning the crystal growth and phase separation. And more importantly, the experiment is done in a very easy setting, making spin-coating and additive annealing in the same step. Therefore, additive annealing is expected to be a new option for the performance enhancement of solution-processed solar cells.

■ ASSOCIATED CONTENT

Supporting Information

The Supporting Information is available free of charge on the ACS Publications website at DOI: 10.1021/acsami.5b06691.

Experimental details and characterization data (PDF)

■ AUTHOR INFORMATION

Corresponding Authors

*E-mail: iamfengliu@gmail.com.
*E-mail: chxbpeng@scut.edu.cn.

Author Contributions

The manuscript was written through contributions of all authors. All authors have given approval to the final version of the manuscript.

Notes

The authors declare no competing financial interest.

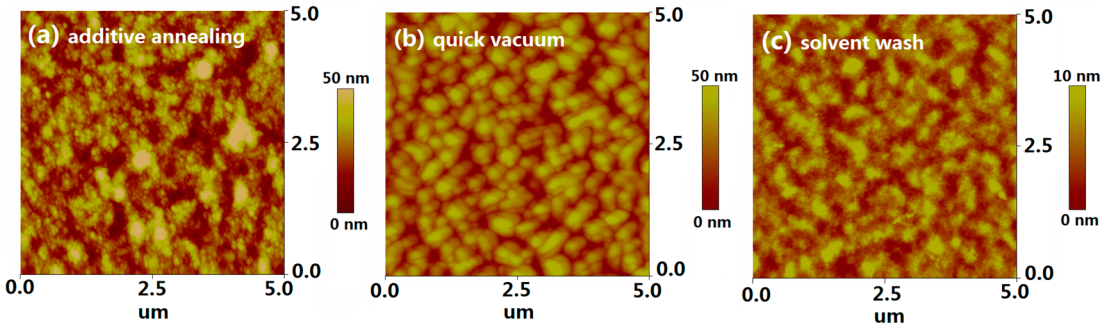

Figure 7. AFM height images of DPPEZnP-O/PCBM BHJ films upon (a) additive annealing, (b) quick vacuuming, and (c) methanol solvent washing.

DOI: 10.1021/acsami.5b06691
ACS Appl. Mater. Interfaces 2015, 7, 21495−21502

■ ACKNOWLEDGMENTS

This work was financially supported by the grants from International Science & Technology Cooperation Program of China (Grants 2013DFG52740, 2010DFA52150) and the National Natural Science Foundation of China (Grants 51473053, 51073060). F.L. and T.P.R. were supported by Polymer-Based Materials for Harvesting Solar Energy (PHaSE), an Energy Frontier Research Center funded by the U.S. Department of Energy, Office of Basic Energy Sciences under Award Number DE-SC0001087. Portions of this research were carried out at beamline 7.3.3 and 11.0.1.2 at the Advanced Light Source, and Molecular Foundary, Lawrence Berkeley National Laboratory, which was supported by the DOE, Office of Science, and Office of Basic Energy Sciences.

■ REFERENCES

(1) Li, Y. N.; Sonar, P.; Murphy, L.; Hong, W. High Mobility Diketopyrrolopyrrole (Dpp)-Based Organic Semiconductor Materials for Organic Thin Film Transistors and Photovoltaics. *Energy Environ. Sci.* **2013**, *6*, 1684−1710.

(2) He, G. R.; Li, Z.; Wan, X. J.; Zhou, J. Y.; Long, G. K.; Zhang, S. Z.; Zhang, M. T.; Chen, Y. S. Efficient Small Molecule Bulk Heterojunction Solar Cells with High Fill Factors Via Introduction of Pi-Stacking Moieties as End Group. *J. Mater. Chem. A* **2013**, *1*, 1801−1809.

(3) Sun, Y. M.; Welch, G. C.; Leong, W. L.; Takacs, C. J.; Bazan, G. C.; Heeger, A. J. Solution-Processed Small-Molecule Solar Cells with 6.7% Efficiency. *Nat. Mater.* **2011**, *11*, 44−48.

(4) Hains, A. W.; Liang, Z. Q.; Woodhouse, M. A.; Gregg, B. A. Molecular Semiconductors in Organic Photovoltaic Cells. *Chem. Rev.* **2010**, *110*, 6689−6735.

(5) He, Z. C.; Zhong, C. M.; Su, S. J.; Xu, M.; Wu, H. B.; Cao, Y. Enhanced Power-Conversion Efficiency in Polymer Solar Cells Using an Inverted Device Structure. *Nat. Photonics* **2012**, *6*, 591−595.

(6) Wei, G. D.; Wang, S. Y.; Sun, K.; Thompson, M. E.; Forrest, S. R. Solvent-Annealed Crystalline Squaraine: Pc70bm (1:6) Solar Cells. *Adv. Energy Mater.* **2011**, *1*, 184−187.

(7) Sharma, G. D.; Daphnomili, D.; Biswas, S.; Coutsolelos, A. G. New Soluble Porphyrin Bearing a Pyridinylethynyl Group as Donor for Bulk Heterojunction Solar Cells. *Org. Electron.* **2013**, *14*, 1811−1819.

(8) Shi, Q. Q.; Cheng, P.; Li, Y. F.; Zhan, X. W. A Solution Processable D-a-D Molecule Based on Thiazolothiazole for High Performance Organic Solar Cells. *Adv. Energy Mater.* **2012**, *2*, 63−67.

(9) Patra, D.; Huang, T. Y.; Chiang, C. C.; Maturana, R. O. V.; Pao, C. W.; Ho, K. C.; Wei, K. H.; Chu, C. W. 2-Alkyl-5-Thienyl-Substituted Benzo[1,2-B:4,5-B ′]Dithiophene-Based Donor Molecules for Solution-Processed Organic Solar Cells. *ACS Appl. Mater. Interfaces* **2013**, *5*, 9494−9500.

(10) Zhang, M. J.; Gu, Y.; Guo, X.; Liu, F.; Zhang, S. Q.; Huo, L. J.; Russell, T. P.; Hou, J. H. Efficient Polymer Solar Cells Based on Benzothiadiazole and Alkylphenyl Substituted Benzodithiophene with a Power Conversion Efficiency over 8%. *Adv. Mater.* **2013**, *25*, 4944−4949.

(11) Liu, Y. H.; Zhao, J. B.; Li, Z. K.; Mu, C.; Ma, W.; Hu, H. W.; Jiang, K.; Lin, H. R.; Ade, H.; Yan, H. Aggregation and Morphology Control Enables Multiple Cases of High-Efficiency Polymer Solar Cells. *Nat. Commun.* **2014**, *5*, 5293.

(12) Chen, Z.; Cai, P.; Chen, J.; Liu, X.; Zhang, L.; Lan, L.; Peng, J.; Ma, Y.; Cao, Y. Low Band-Gap Conjugated Polymers with Strong Interchain Aggregation and Very High Hole Mobility Towards Highly Efficient Thick-Film Polymer Solar Cells. *Adv. Mater.* **2014**, *26*, 2586−2591.

(13) Gupta, V.; Kyaw, A. K.; Wang, D. H.; Chand, S.; Bazan, G. C.; Heeger, A. J. Barium: An Efficient Cathode Layer for Bulk-Heterojunction Solar Cells. *Sci. Rep.* **2013**, *3*, 1965.

(14) Kan, B.; Zhang, Q.; Li, M. M.; Wan, X. J.; Ni, W.; Long, G. K.; Wang, Y. C.; Yang, X.; Feng, H. R.; Chen, Y. S. Solution-Processed Organic Solar Cells Based on Dialkylthiol-Substituted Benzodithiophene Unit with Efficiency near 10%. *J. Am. Chem. Soc.* **2014**, *136*, 15529−15532.

(15) Huang, Y.; Li, L.; Peng, X.; Peng, J.; Cao, Y. Solution Processed Small Molecule Bulk Heterojunction Organic Photovoltaics Based on a Conjugated Donor-Acceptor Porphyrin. *J. Mater. Chem.* **2012**, *22*, 21841−21844.

(16) Qin, H.; Li, L.; Guo, F.; Su, S.; Peng, J.; Cao, Y.; Peng, X. Solution-Processed Bulk Heterojunction Solar Cells Based on a Porphyrin Small Molecule with 7% Power Conversion Efficiency. *Energy Environ. Sci.* **2014**, *7*, 1397−1401.

(17) Gao, K.; Li, L.; Lai, T.; Xiao, L.; Huang, Y.; Huang, F.; Peng, J.; Cao, Y.; Liu, F.; Russell, T. P.; Janssen, R. A. J.; Peng, X. Deep Absorbing Porphyrin Small Molecule for High-Performance Organic Solar Cells with Very Low Energy Losses. *J. Am. Chem. Soc.* **2015**, *137*, 7282−7285.

(18) Kumar, C. V.; Cabau, L.; Koukaras, E. N.; Sharma, G. D.; Palomares, E. Synthesis, Optical and Electrochemical Properties of the A-Pi-D-Pi-A Porphyrin and Its Application as an Electron Donor in Efficient Solution Processed Bulk Heterojunction Solar Cells. *Nanoscale* **2015**, *7*, 179−189.

(19) Kumar, C. V.; Cabau, L.; Koukaras, E. N.; Sharma, A.; Sharma, G. D.; Palomares, E. A-Pi-D-Pi-a Based Porphyrin for Solution Processed Small Molecule Bulk Heterojunction Solar Cells. *J. Mater. Chem. A* **2015**, *3*, 16287−16301.

(20) Campoy-Quiles, M.; Ferenczi, T.; Agostinelli, T.; Etchegoin, P. G.; Kim, Y.; Anthopoulos, T. D.; Stavrinou, P. N.; Bradley, D. D. C.; Nelson, J. Morphology Evolution Via Self-Organization and Lateral and Vertical Diffusion in Polymer: Fullerene Solar Cell Blends. *Nat. Mater.* **2008**, *7*, 158−164.

(21) Chen, L. M.; Hong, Z. R.; Li, G.; Yang, Y. Recent Progress in Polymer Solar Cells: Manipulation of Polymer: Fullerene Morphology and the Formation of Efficient Inverted Polymer Solar Cells. *Adv. Mater.* **2009**, *21*, 1434−1449.

(22) Zou, J. Y.; Yip, H. L.; Zhang, Y.; Gao, Y.; Chien, S. C.; O′Malley, K.; Chueh, C. C.; Chen, H. Z.; Jen, A. K. Y. High-Performance Inverted Polymer Solar Cells: Device Characterization, Optical Modeling, and Hole-Transporting Modifications. *Adv. Funct. Mater.* **2012**, *22*, 2804−2811.

(23) Huang, Y.; Kramer, E. J.; Heeger, A. J.; Bazan, G. C. Bulk Heterojunction Solar Cells: Morphology and Performance Relationships. *Chem. Rev.* **2014**, *114*, 7006−7043.

(24) Verploegen, E.; Miller, C. E.; Schmidt, K.; Bao, Z. N.; Toney, M. F. Manipulating the Morphology of P3ht-Pcbm Bulk Heterojunction Blends with Solvent Vapor Annealing. *Chem. Mater.* **2012**, *24*, 3923−3931.

(25) Li, G.; Yao, Y.; Yang, H.; Shrotriya, V.; Yang, G.; Yang, Y. "Solvent Annealing" Effect in Polymer Solar Cells Based on Poly(3-Hexylthiophene) and Methanofullerenes. *Adv. Funct. Mater.* **2007**, *17*, 1636−1644.

(26) Dang, M. T.; Wuest, J. D. Using Volatile Additives to Alter the Morphology and Performance of Active Layers in Thin-Film Molecular Photovoltaic Devices Incorporating Bulk Heterojunctions. *Chem. Soc. Rev.* **2013**, *42*, 9105−9126.

(27) Sun, Y. M.; Welch, G. C.; Leong, W. L.; Takacs, C. J.; Bazan, G. C.; Heeger, A. J. Solution-Processed Small-Molecule Solar Cells with 6.7% Efficiency. *Nat. Mater.* **2012**, *11*, 44−48.

(28) Su, M. S.; Kuo, C. Y.; Yuan, M. C.; Jeng, U. S.; Su, C. J.; Wei, K. H. Improving Device Efficiency of Polymer/Fullerene Bulk Heterojunction Solar Cells through Enhanced Crystallinity and Reduced Grain Boundaries Induced by Solvent Additives. *Adv. Mater.* **2011**, *23*, 3315−3319.

(29) Li, Z.; Tsang, S. W.; Du, X. M.; Scoles, L.; Robertson, G.; Zhang, Y. G.; Toll, F.; Tao, Y.; Lu, J. P.; Ding, J. F. Alternating Copolymers of Cyclopenta[2,1-B;3,4-B ′] Dithiophene and Thieno-[3,4-C]Pyrrole-4,6-Dione for High-Performance Polymer Solar Cells. *Adv. Funct. Mater.* **2011**, *21*, 3331−3336.

DOI: 10.1021/acsami.5b06691
ACS Appl. Mater. Interfaces 2015, 7, 21495−21502

(30) Liu, F.; Zhao, W.; Tumbleston, J. R.; Wang, C.; Gu, Y.; Wang, D.; Briseno, A. L.; Ade, H.; Russell, T. P. Understanding the Morphology of Ptb7: Pcbm Blends in Organic Photovoltaics. *Adv. Energy Mater.* **2014**, *4*, 1301377.
(31) Lee, J. K.; Ma, W. L.; Brabec, C. J.; Yuen, J.; Moon, J. S.; Kim, J. Y.; Lee, K.; Bazan, G. C.; Heeger, A. J. Processing Additives for Improved Efficiency from Bulk Heterojunction Solar Cells. *J. Am. Chem. Soc.* **2008**, *130*, 3619−3623.
(32) Guo, X. G.; Zhou, N. J.; Lou, S. J.; Smith, J.; Tice, D. B.; Hennek, J. W.; Ortiz, R. P.; Navarrete, J. T. L.; Li, S. Y.; Strzalka, J.; Chen, L. X.; Chang, R. P. H.; Facchetti, A.; Marks, T. J. Polymer Solar Cells with Enhanced Fill Factors. *Nat. Photonics* **2013**, *7*, 825−833.
(33) Chang, L. L.; Lademann, H. W. A.; Bonekamp, J. B.; Meerholz, K.; Moule, A. J. Effect of Trace Solvent on the Morphology of P3ht:Pcbm Bulk Heterojunction Solar Cells. *Adv. Funct. Mater.* **2011**, *21*, 1779−1787.
(34) Xiao, Z.; Yuan, Y.; Yang, B.; VanDerslice, J.; Chen, J.; Dyck, O.; Duscher, G.; Huang, J. Universal Formation of Compositionally Graded Bulk Heterojunction for Efficiency Enhancement in Organic Photovoltaics. *Adv. Mater.* **2014**, *26*, 3068−3075.
(35) Ye, L.; Jing, Y.; Guo, X.; Sun, H.; Zhang, S. Q.; Zhang, M. J.; Huo, L. J.; Hou, J. H. Remove the Residual Additives toward Enhanced Efficiency with Higher Reproducibility in Polymer Solar Cells. *J. Phys. Chem. C* **2013**, *117*, 14920−14928.
(36) Subbiah, J.; Amb, C. M.; Irfan, I.; Gao, Y. L.; Reynolds, J. R.; So, F. High-Efficiency Inverted Polymer Solar Cells with Double Interlayer. *ACS Appl. Mater. Interfaces* **2012**, *4*, 866−870.
(37) Yang, T. B.; Wang, M.; Duan, C. H.; Hu, X. W.; Huang, L.; Peng, J. B.; Huang, F.; Gong, X. Inverted Polymer Solar Cells with 8.4% Efficiency by Conjugated Polyelectrolyte. *Energy Environ. Sci.* **2012**, *5*, 8208−8214.
(38) Hau, S. K.; Yip, H. L.; Baek, N. S.; Zou, J. Y.; O′Malley, K.; Jen, A. K. Y. Air-Stable Inverted Flexible Polymer Solar Cells Using Zinc Oxide Nanoparticles as an Electron Selective Layer. *Appl. Phys. Lett.* **2008**, *92*, 253301.
(39) Harschneck, T.; Zhou, N. J.; Manley, E. F.; Lou, S. J.; Yu, X. G.; Butler, M. R.; Timalsina, A.; Turrisi, R.; Ratner, M. A.; Chen, L. X.; Chang, R. P. H.; Facchetti, A.; Marks, T. J. Substantial Photovoltaic Response and Morphology Tuning in Benzo[1,2-B:6,5-B ′]-Dithiophene (Bbdt) Molecular Donors (Vol 50, Pg 4099, 2014). *Chem. Commun.* **2014**, *50*, 4099−4101.
(40) Servaites, J. D.; Yeganeh, S.; Marks, T. J.; Ratner, M. A. Efficiency Enhancement in Organic Photovoltaic Cells: Consequences of Optimizing Series Resistance. *Adv. Funct. Mater.* **2010**, *20*, 97−104.
(41) Walker, B.; Tamayo, A. B.; Dang, X. D.; Zalar, P.; Seo, J. H.; Garcia, A.; Tantiwiwat, M.; Nguyen, T. Q. Nanoscale Phase Separation and High Photovoltaic Efficiency in Solution-Processed, Small-Molecule Bulk Heterojunction Solar Cells. *Adv. Funct. Mater.* **2009**, *19*, 3063−3069.
(42) Gao, J.; Chen, W.; Dou, L.; Chen, C.-C.; Chang, W.-H.; Liu, Y.; Li, G.; Yang, Y. Elucidating Double Aggregation Mechanisms in the Morphology Optimization of Diketopyrrolopyrrole-Based Narrow Bandgap Polymer Solar Cells. *Adv. Mater.* **2014**, *26*, 3142−3147.
(43) Wu, Z. W.; Song, T.; Jin, Y. Z.; Sun, B. Q. High Performance Solar Cell Based on Ultra-Thin Poly(3-Hexylthiophene): Fullerene Film without Thermal and Solvent Annealing. *Appl. Phys. Lett.* **2011**, *99*, 143306.

DOI: 10.1021/acsami.5b06691
ACS Appl. Mater. Interfaces 2015, 7, 21495−21502